ACS Catalysis

Research Article

Cite This: ACS Catal. 2018, 8, 3999−4008

pubs.acs.org/acscatalysis

Examination of Near-Electrode Concentration Gradients and Kinetic Impacts on the Electrochemical Reduction of CO_2 using Surface-Enhanced Infrared Spectroscopy

Marco Dunwell, Xuan Yang, Brian P. Setzler, Jacob Anibal, Yushan Yan,* and Bingjun Xu*

Center for Catalytic Science and Technology, Department of Chemical and Biomolecular Engineering, University of Delaware, Newark, Delaware 19716, United States

Supporting Information

ABSTRACT: Localized concentration gradients within the electrochemical double layer during various electrochemical processes can have wide-ranging impacts; however, experimental investigation to quantitatively correlate the rate of surface-mediated electrochemical reaction with the interfacial species concentrations has historically been lacking. In this work, we demonstrate a spectroscopic method for the in situ determination of the surface pH using the CO_2 reduction reaction as a model system. Attenuated total reflectance surface-enhanced infrared absorption spectroscopy is employed to monitor the ratio of vibrational bands of carbonate and bicarbonate as a function of electrode potential. Integrated areas of vibrational bands are then compared with those obtained from calibration spectra collected in electrolytes with known pH values to determine near-electrode proton concentrations. Experimentally determined interfacial proton concentrations are then related to the resultant concentration overpotentials to examine their impact on electrokinetics. We show that, in CO_2-saturated sodium bicarbonate solutions, a concentration overpotential of over 150 mV can be induced during electrolysis at −1.0 V vs RHE, leading to substantial losses in energy efficiency. We also show that increases in both convection and buffering capacity of the electrolyte can mitigate interfacial concentration gradients. On the basis of these results, we further discuss how increases in concentration overpotential affect the mechanistic interpretations of the CO_2 reduction electrocatalysis, particularly in terms of Tafel slopes and reaction orders.

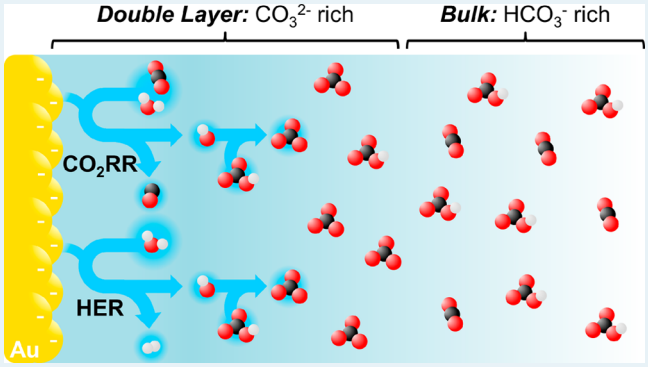

KEYWORDS: *surface pH, concentration overpotential, attenuated total reflectance surface-enhanced infrared absorption spectroscopy, CO_2 reduction, near surface concentration*

INTRODUCTION

The phenomenon of localized changes in electrolyte concentrations near electrode surfaces relative to those in the bulk during electrolysis is well-understood[1] and has been proven to have significant impacts on a wide variety of electrochemical processes.[2−24] During electrodeposition of Ni and Co for example, increases in $[OH^-]$ due to the accompanying hydrogen evolution reaction (HER) can lead to precipitation of undesired, insoluble metal hydroxides, which can cause undesired changes in the physical or chemical properties of the electrodeposited layer.[5,11,19,20] Similarly, during the anodic passivation of Zn, decreases in $[OH^-]$ can induce a positive shift in the equilibrium potential of the oxidation, thereby requiring additional overpotential for the formation of ZnO rather than soluble hydroxides.[4] Aside from changes to the chemical environment, concentration gradients in the diffuse layer can lead to mass-transport limitations, thereby influencing electrokinetics as described by the Nernst−Planck equation.[1] For example, changes in interfacial $[H^+]$ and $[OH^-]$ have been shown to significantly impact rates of important electrochemical processes such as hydrogen evolution and oxidation as well as oxygen and hydrogen peroxide reduction via corresponding increases in concentration overpotential (η_c).[3,12,23]

The η_c, defined here as the additional overpotential arising from the change in near-electrode concentrations relative to the bulk due to interfacial concentration gradients, is particularly large when these reactions are conducted at intermediate pH values, where relatively small changes in $[H^+]$ or $[OH^-]$ can cause significant η_c.[12] Strongly acidic or alkaline electrolytes are more resilient to η_c as much larger absolute changes in $[H^+]$ or $[OH^-]$ are required to substantially change the equilibrium potential based on the exponential dependence of the equilibrium potential on reactant concentrations in the Nernst equation. Using a simplified example, consider a closed 100 μm diffusion layer and a planar electrode with a geometric area of 1 cm^2 operating at −1 mA cm^{-2} for 10 s so that ∼0.1 μmol OH^-

Received: March 14, 2018
Published: April 3, 2018

DOI: 10.1021/acscatal.8b01032
ACS Catal. 2018, 8, 3999−4008

is produced. If the initial electrolyte pH is 1, the $[H^+]$ will decrease from 0.1 to 0.09 M, resulting in an average pH within the diffusion layer of 1.05, which corresponds to a $\eta_c < 3$ mV. Conversely, if the initial electrolyte pH is 7, the final pH in the diffusion layer would be 8, corresponding to a $\eta_c = 59$ mV for a reaction that is first order in $[H^+]$. Despite the theoretical and demonstrated impact of η_c changes due to the near-electrode accumulation/depletion of $[H^+]$ or $[OH^-]$, the effects are generally ignored due to the difficulty of reliably quantifying η_c. Although various experimental methods have been employed to measure and account for the concentration gradients that drive η_c, they generally suffer from poor precision, require destructive techniques, or are limited to specific electrochemical systems.[5,7,8,10,11,13]

The topic of interfacial concentration gradients, and the resultant increase in η_c, is of particular interest in studies of CO_2 (CO_2RR) and CO (CORR) reduction reactions in which one OH^- ion is produced at the cathode for every e^- transferred in either the desired reaction (with the exception of formate in which 1 OH^- is produced for every 2 e^-) or in the competing hydrogen evolution reaction (HER).[9] As CO_2 reduction typically takes place in near neutral pH electrolytes (pH ~7), production of OH^- leads to larger η_c than reactions conducted in more acidic and alkaline environments.[12] Hori et al. first investigated the effects of current-induced concentration gradients by calculating near-electrode concentrations in various buffer solutions during the CO_2RR and CORR on Cu cathodes.[10,25] The initial findings were correlated to the experimentally observed increases in CO production rate during the CO_2RR, and increased selectivity toward ethylene and alcohols during the CORR in unbuffered or weakly buffered electrolytes were attributed to the suppression of HER by an increase in the required η_c for the HER due to elevated $[OH^-]$ near the electrode. Gupta et al. conducted a more rigorous theoretical treatment of these concentration gradients during the CO_2RR in which near-electrode concentrations were simulated at different current densities, total $KHCO_3$ concentrations, and stirring rates.[6] Moreover, the authors emphasized the importance of accounting for these concentration gradients during the CO_2RR, particularly in mechanistic work by relating Tafel slope changes to local $[H^+]$ gradients. Reactivity studies of CO_2 reduction on Cu at different rotation rates using a rotating disk electrode also confirm that increases in $[OH^-]$ correspond to enhanced CO_2RR selectivity.[14] A recent work by Raciti et al. coupled reactivity studies with theoretical treatments of the interfacial concentrations for nanostructured electrodes and concluded that an interfacial pH of 9−10 is optimal for C_2 production by suppressing the HER while maintaining dissolved CO_2 concentrations near the electrode.[26] Conversely, Singh et al. proposed that hydrolysis of water in the hydration sphere of cations acts as a buffer against interfacial concentration gradients at potentials below 1.0 V vs RHE during the CO_2RR on both Ag and Cu cathodes.[21,27] Contrary to the claims by Hori and Murata, Singh proposed that the mitigation of near electrode concentration gradients by cation hydrolysis improves selectivity of the CO_2RR over the HER by maintaining dissolved CO_2 ($CO_{2(aq)}$) concentrations near the cathode. Ayemoba et al. used attenuated total reflectance surface-enhanced infrared absorption spectroscopy (ATR-SEIRAS) to experimentally confirm these effects. However, the conditions at which spectroscopic investigations were conducted do not reflect those in reactivity studies (no stirring), and thus, the results are inconclusive.[2]

Although changes in near-electrode concentrations are generally believed to influence both reaction rates and selectivity through the corresponding changes to η_c, until recently, only theoretical estimates of local concentration gradients during the CO_2RR have been made.[6,21,25,28] Furthermore, rigorous connections between current-induced concentration gradients and electrode kinetics are lacking. In this work, we employ ATR-SEIRAS, which allows for the selective observation of near-electrode species to experimentally quantify current-induced concentration gradients as a function of reaction rate on Au film electrodes under typical reaction conditions.[29−32] The term "near-electrode" in this work therefore refers to the 5−10 nm region sampled by ATR-SEIRAS weighted to the region closer to the electrode based on the strength of the evanescent IR wave sampling the electrolyte. In turn, near-electrode concentration gradients are then related to increases in η_c for the CO_2RR based on the rate expression for the CO_2RR to CO. It is important to note that changes in interfacial concentrations are a function of geometric current density, rather than potential, and are likely to be similar on different electrode materials despite changes in product selectivity (with the exception of formate). Both the HER and the CO_2RR produce one equivalent of OH^- for each e^- transfer such that current-induced concentration gradients rely primarily on the geometric current density of the reaction and are largely independent of electrode material and reaction selectivity. It should be noted, however, that product selectivity between gas and liquid products could cause differences in interfacial concentrations due to convection arising from gas bubble formation, especially when the electrolyte is unstirred. As a result, although the quantitative relationships between η_c and geometric current density established in this work under each set of reaction conditions are likely to be similar on any bulk electrode material that exhibits a first order dependence on $[H^+]$, provided electrolyte composition and convection are equal, exact quantitative relationships should be established for each electrode material using the method outlined in this work.

MATERIALS AND METHODS

Materials. ATR-SEIRAS experiments were conducted in two custom spectroelectrochemical cells. Spectroscopic measurements in 0.25 and 1.0 M $NaHCO_3$ were collected in a cell described in our previous work.[33] Experiments in 0.5 M $NaHCO_3$ were conducted in a newly designed spectroelectrochemical cell in which the Si ATR crystal is mounted on the side of the cell, which allows for stirring of the electrolyte using a magnetic stir bar (Figure 1). In practice, both cells are the same when not stirred, such that data from experiments at each concentration from these two cells can be directly compared. The ability to monitor reactions under convection represents a significant step forward in the *operando* investigation of electrochemical processes. In typical external reflection techniques, such as subtractively normalized interfacial Fourier Transform infrared spectroscopy, transport is severely hampered by the thin-layer electrolyte configuration. Although the use of ATR-SEIRAS improves transport drastically, transport was still governed solely by diffusion in all previous spectroelectrochemical studies.[30] A polycrystalline Au film, chemically deposited on the reflecting plane of a Si prism, was used as the working electrode.[33] A graphite rod, rather than Pt, counter electrode was used for all experiments to prevent contamination of the Au working electrode by dissolved Pt originating from the counter electrode.[33] A Ag/AgCl (3.0 M

DOI: 10.1021/acscatal.8b01032
ACS Catal. 2018, 8, 3999−4008

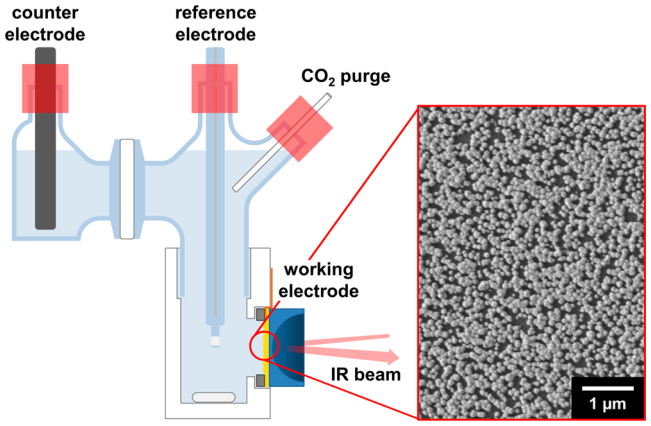

Figure 1. Stirred spectroscopic cell used for all measurements in 0.5 M $NaHCO_3$ with Au film working electrode, graphite rod counter electrode, and Ag/AgCl reference electrodes. Inset: A scanning electron microscope image of the Au film on Si.

KCl, BASi) reference electrode was used for all experiments. $NaHCO_3$ electrolytes were prepared by purging a solution made from Na_2CO_3 (Fluka, >99.9999%) overnight with high purity CO_2 gas (Matheson, 99.999%) until the solution pH no longer decreased, indicating full conversion of Na_2CO_3 to $NaHCO_3$.[33,34] The electrolyte was purified using a solid-supported iminodiacetate resin (Chelex 100, Sigma-Aldrich) to prevent any potential impurity metal deposition and achieve a sustainable catalytic surface during the CO_2RR.[35] All spectroscopic measurements were collected with 4 cm^{-1} resolution and at least 128 coadded scans using an Agilent Technologies Cary 660 FTIR spectrometer equipped with a liquid nitrogen-cooled MCT detector. A Pike Technologies VeeMAX II ATR accessory was used for experiments in 0.25 and 1.0 M $NaHCO_3$, whereas a customized ATR setup using optical components from ThorLabs was used with the stirred spectroelectrochemical cell. Electrochemical measurements were conducted using a Solartron SI 1260/1287 system. Impedance measurements were conducted at the beginning of each experiment, and the internal resistance (typically 20−30 Ω) was actively corrected for throughout all experiments. Spectra are presented in absorbance where positive and negative peaks signify an increase and decrease in the corresponding interfacial species, respectively. All potentials are given on the reversible hydrogen electrode (RHE) scale unless noted otherwise.

Quantification of Changes in Concentration Overpotential. The magnitude of η_c at the electrode due to OH^- formation was quantified using ATR-SEIRAS in which the pH near the electrode was estimated using the ratio of solution phase carbonate and bicarbonate peaks at 1400 and 1363 cm^{-1} (which are governed by equilibria among CO_2, bicarbonate, carbonate, and hydroxide), respectively (Figure S1).[36] η_c arising from OH^- formation was calculated via eq 1 derived from the rate expression for the CO_2RR on Au electrodes as detailed in the Supporting Information. Subscripts "I" and "B" refer to interfacial and bulk values, respectively.

$$\eta_c = \frac{2.3RT}{F}\log\left(\frac{[CO_{2(aq)}]_B[H^+]_B}{[CO_{2(aq)}]_I[H^+]_I}\right) \quad (1)$$

In each experiment, the Au film was pretreated by potential cycling between −0.4 and 1.0 V in 0.1 M $HClO_4$ under 1 atm Ar to activate the surface enhancement effect and settle the Au film electrode. After pretreatment, the electrochemical cell was triple-rinsed and refilled using high-purity distilled water in which the background spectrum was collected. It is imperative to collect the background in a (bi)carbonate free solution to ensure that the entirety of the carbonate and bicarbonate bands are accounted for in the sample spectra. Following background collection, the electrochemical cell was filled with 0.25, 0.5, or 1.0 M of CO_2-saturated $NaHCO_3$. The electrode potential was then stepped down to either −1.0 (in 0.25 M $NaHCO_3$) or −0.9 V (in 0.5 and 1.0 M $NaHCO_3$) without collecting spectra. The lower potential bounds used in this study represent the lowest potential that the working electrodes were able to sustain without rupture due to excessive HER in each electrolyte. After holding at the lowest potential for at least 1 min to ensure sufficient robustness of the film, the potential was stepped from 1.0 V to the minimum potential in 0.1 V increments with spectra collected at each increment after the current roughly stabilized. Although the current on low surface area Au electrodes consistently decays slowly under potentiostatic conditions, after ∼1 min at each potential step, the decay slows significantly such that capacitive current no longer contributes and the current changes less than 6% during the 1 min that the spectra are collected. In the case of 0.5 M $NaHCO_3$, spectra were collected at each potential both in the absence and presence of stirring (1800 rpm). Calibration spectra were then collected on the same Au film to ensure the accuracy of each calibration for each experiment by eliminating the variance in penetration depth between films.

The calibration spectra were collected at various bulk pH values at 0.1 V. The electrolyte pH (and equilibrated species concentrations) was varied by adding aliquots of NaOH matching the concentration of each starting bicarbonate concentration (so that the total Na^+ concentration remained constant) to ensure no changes in total (bi)carbonate concentration. Bulk pH values were measured using a pH meter after equilibration of the pH following each addition of NaOH. Calibration spectra were typically collected in pH increments of ∼0.2 units. The potential during the calibration was chosen at 0.1 V to ensure that the calibration spectra were free from bands associated with both adsorbed carbonate (which appear above 0.4 V) while maintaining minimal current so that concentration gradients were negligible.[33]

Near-electrode concentrations were then obtained by fitting the bands associated with carbonate (∼1400 cm^{-1}) and bicarbonate (∼1362 cm^{-1}) in both the sample spectra (collected as a function of potential) and calibration spectra (collected as a function of bulk pH without any current), finding the ratio between the bicarbonate peak area and carbonate peak area, and correlating that ratio in the sample spectra to those in the calibration spectra of known pH (Figure S1).[36] Linear interpolation of ratios between pH increments of the calibration spectra was used to determine near-electrode concentrations as a function of electrode potential, and the portion of η_c due to changes in $[H^+]$ assuming dissolved CO_2 (referred to as $CO_{2(aq)}$ below) concentration is constant (η_{c,H^+}) was calculated using eq 1 based on the $[H^+]$ gradient between the bulk and near-electrode region.

Determination of Dissolved CO_2 Concentrations. Dissolved CO_2 concentrations along with the resultant η_c due to changes in $[CO_{2(aq)}]$ (η_{c,CO_2}) were determined in 0.5 M $NaHCO_3$ both with and without stirring via ATR-SEIRAS

DOI: 10.1021/acscatal.8b01032
ACS Catal. 2018, 8, 3999−4008

Table 1. Rate Constants at 298.15 K for Carbonate Equilibrium Reactions from Ref 39

reaction	k_+	k_-
$CO_2 + H_2O \rightleftharpoons HCO_3^- + H^+$	3.71×10^{-2} s^{-1}	2.67×10^{4} kg mol^{-1} s^{-1}
$CO_2 + OH^- \rightleftharpoons HCO_3^-$	2.23×10^{3} kg mol^{-1} s^{-1}	9.71×10^{-5} s^{-1}
$HCO_3^- + OH^- \rightleftharpoons CO_3^{2-} + H_2O$	6.0×10^{9} kg mol^{-1} s^{-1}	3.06×10^{5} s^{-1}

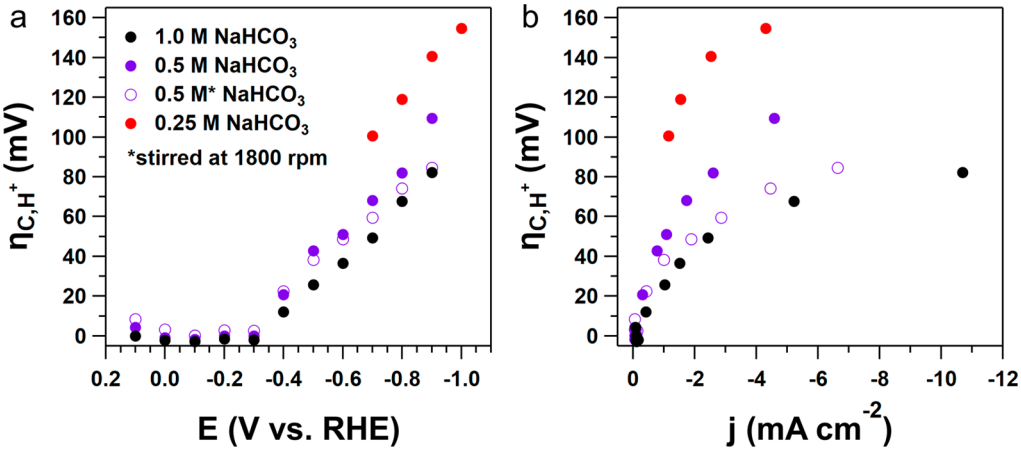

Figure 2. η_{c,H^+} versus (a) electrode potential and (b) current density in CO_2-saturated 0.25 (red), 0.5 (purple), and 1.0 M (black) $NaHCO_3$ with (open circles) and without (solid circles) stirring.

using a similar method to that described in determining η_{c,H^+} due to changes in interfacial [H^+] gradients (Figure S2). The Au film was first cycled in Ar-saturated 0.5 M $NaHCO_3$ from −0.4 to 1.0 V to pretreat the electrode. A background spectrum was then collected at 0.0 V in the Ar-saturated electrolyte to ensure the absence of dissolved CO_2 in the background. The electrolyte was then saturated under 1 atm CO_2 for sample spectra collection. The electrode potential was first held at 0.0 V, and the initial sample spectrum was collected after which the potential was swept at 2 mV s^{-1} to −0.1 V at which the potential was held while another spectrum was collected. Next, the potential was swept at 10 mV s^{-1} back to 0.0 V, where another spectrum was collected. This process was repeated in 0.1 V increments from 0.0 to −0.9 V. Slow scans to each potential (rather than large potential steps, which lead to large capacitive currents) were employed to maintain the stability of the film over the course of the experiment. Spectra were collected at 0.0 V after each sample potential to account for changes in sampling depth over the course of the experiment arising from slow changes in the Au film electrode. $CO_{2(aq)}$ concentrations were then determined by taking the ratio of the peak area at each potential and the peak area from the following spectrum at 0.0 V, and multiplying by the known bulk $CO_{2(aq)}$ concentration. The entire experiment was completed twice: once without convection and again under stirring from a small stir bar at 1800 rpm. In the stirred experiment, spectra were collected at −0.7 V at stir rates of 0, 450, 900, 1350, and 1800 rpm to examine the effect of different levels of convection.

It is important to emphasize the differences between the experimental methods used in this work and those of previous estimations of current-induced concentration gradients using ATR-SEIRAS. Specifically, Ayemoba et al. quantified near-electrode concentration gradients by monitoring the change in $CO_{2(aq)}$ and bicarbonate band intensity and correlating the change in this ratio directly to changes in pH near the electrode.[2] This approach has two primary deficiencies: (1) because of the slow kinetics of hydration relative to transport (particularly with convection) of $CO_{2(aq)}$, the $CO_{2(aq)}$ concentration is largely independent of interfacial concentration gradients under typical reaction conditions (as shown in the next section),[6,37] and (2) by taking the ratio of band intensity, rather than area, the change in the ratio will be underestimated as area scales roughly with the square of the peak intensity. In contrast, in this work concentration gradients are measured using the relative peak areas of aqueous carbonate and bicarbonate bands (which remain in equilibrium throughout the reaction), whereas the $CO_{2(aq)}$ band is considered partially independent of the concentration of other electrolyte species due to the relatively slow kinetics of the CO_2 bicarbonate equilibrium (Table 1).[38,39]

RESULTS AND DISCUSSION

Impact of OH^- Formation on η_{c,H^+}. Experimental quantification of η_{c,H^+} via ATR-SEIRAS reveals that η_{c,H^+} increases almost linearly with decreasing potential below −0.3 V (Figure 2a), where the current begins to increase appreciably. The magnitudes of observed η_{c,H^+} are large enough to significantly impact the kinetics of the CO_2RR under typical reaction conditions, assuming the rate-determining step for CO_2 reduction involves or is preceded by a proton transfer step as previously proposed.[33,40−44] For example, in 0.5 M $NaHCO_3$ without stirring (Figure 2a, solid purple), a η_{c,H^+} of 68 mV is observed so that the kinetic overpotential is the difference between the total applied overpotential and η_{c,H^+}, which increases with current density.

The concentration of the electrolyte, and particularly the strength of the buffer, has a strong impact on the magnitude of η_{c,H^+}. Concentration of bicarbonate exerts two competing effects on η_{c,H^+} in CO_2RR: (1) an increase in concentration should be expected to suppress near-electrode concentration changes and therefore η_{c,H^+} due to the stronger buffering capacity of the electrolyte, and (2) the promotional effect of bicarbonate on the CO_2RR with a reported reaction order of ∼1 leads to an increase in the rate of the CO_2RR, driving larger

DOI: 10.1021/acscatal.8b01032
ACS Catal. 2018, 8, 3999−4008

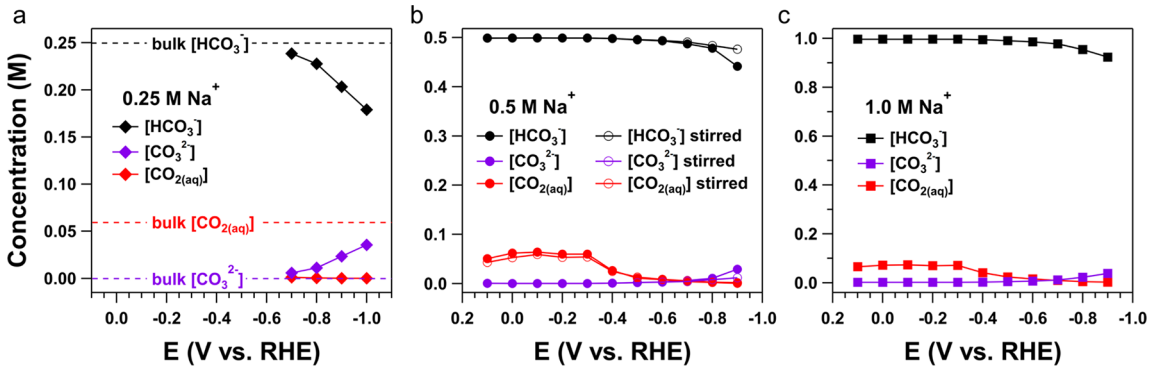

Figure 3. Calculated $CO_{2(aq)}$ (red), bicarbonate (black), and carbonate (purple) near-surface concentrations versus uncorrected potential in CO_2-saturated (a) 0.25, (b) 0.5, and (c) 1.0 M $NaHCO_3$. Concentrations are calculated assuming equilibrium among $CO_{2(aq)}$, HCO_3^-, and CO_3^{2-}.

concentration gradients and therefore an increase in η_{c,H^+}.[33] To evaluate the relative magnitude of these two countervailing effects, η_{c,H^+} was determined in CO_2-saturated 0.25, 0.5, and 1.0 M $NaHCO_3$ as a function of electrode potential. Comparing the η_{c,H^+} at the same potential of −0.9 V, 0.25 M shows the largest η_{c,H^+} (141 mV) followed by 0.5 M (η_{c,H^+} = 109 mV) and 1.0 M (η_{c,H^+} = 82 mV). This trend suggests that, despite the positive correlation between the current and $NaHCO_3$ concentration, the increase in buffering capacity effectively mitigates interfacial concentration changes and thereby decreases η_{c,H^+}. Because the OH^- production rate drives increases in η_{c,H^+}, it may be more informative to plot η_{c,H^+} vs current density than the electrode potential (Figure 2b). Higher $NaHCO_3$ concentration has a more pronounced effect on mitigating the growth of η_{c,H^+} at the same current density; e.g., at −5 mA/cm^2, η_{c,H^+} in 0.25 M is more than twice that in 1 M $NaHCO_3$ electrolyte. This difference is because the promotional effect of a higher $NaHCO_3$ concentration on the electrode reaction rate is absent at the same current density while the mitigating effect of a higher buffering capacity remains.

A custom spectroelectrochemical cell capable of stirring was employed to investigate the effect of convection on η_{c,H^+} (Figure 1). In contrast to the conventional SEIRAS cells in which the working electrode is located at the bottom, we designed and constructed a spectroelectrochemical cell with the ATR crystal mounted at the side, thus allowing magnetic stirring at the bottom of the cell. In the 0.5 M $NaHCO_3$ experiment, spectra were collected at each potential both without and with stirring at 1800 rpm. Similar to increasing concentration, stirring has two competing effects. Elevation of η_{c,H^+} is expected to be mitigated with stirring by improving transport of both $CO_{2(aq)}$ and bicarbonate (which neutralize OH^-) toward and carbonate away from the electrode. Conversely, improved transport through convection also increases current density at a given potential, driving larger η_{c,H^+} values. Experiments show that, with stirring, η_{c,H^+} is significantly decreased at lower potentials relative to the unstirred case. Comparing again at −0.90 V, η_{c,H^+} = 109 mV without stirring, whereas η_{c,H^+} = 84 mV when the solution is stirred at 1800 rpm, yielding an increase in the kinetic overpotential of 25 mV under stirring (Figure 2b, open circles). Again, the trend demonstrates that improved transport due to convection is more effective in reducing η_{c,H^+} than the competing effect caused by the increase in current density.

Importantly, the experimentally determined near-electrode concentrations (summarized as surface pH in Figures S3−S6) are in good agreement with the calculations of Gupta et al., suggesting that modeling may be an efficient method of estimating interfacial concentration gradients (and their impact on kinetics) for electrochemical processes.[6] We would like to note here that, although in this work changes in concentration near the electrode are generally referred to as "near-electrode" or "interfacial" concentration gradients, these changes are often referred to as localized, interfacial, or surface pH changes in the existing literature.[2,6,11,12,21,26] For ease of comparison, the spectroscopic measurements in this work can also be presented in terms of surface pH (Figure S3−S6). Following this pattern, the change in concentration overpotential arising from $[H^+]$ gradients, referred to in this work as η_{c,H^+}, is analogous to a change in electrode potential on the RHE scale. As the pH of the electrolyte increases near the electrode, the potential vs RHE decreases by 59 mV pH^{-1} as defined by eq 2, so that the value of η_{c,H^+} can alternatively be considered as an overestimation of applied potential on an RHE scale.

$$E_{RHE} = E_{SHE} + \frac{2.3RT}{F}\text{pH} \quad (2)$$

Using this perspective, we observe that the surface pH changes in CO_2-saturated 0.25, 0.5, and 1.0 M $NaHCO_3$ electrolytes at rates of 1.58, 1.15, and 0.81 pH units per decade of current density, respectively, for unstirred electrolytes, and 0.82 pH units per decade in 0.5 M $NaHCO_3$ when stirred at 1800 rpm.

Near-Surface Concentrations. In addition to incurring substantial η_{c,H^+}, production of hydroxide ions also causes deviations in the concentration of various species near the electrode surface from their expected bulk equilibrium values. Concentration of $CO_{2(aq)}$ near the electrode with and without stirring as a function of potential was calculated using the experimentally determined interfacial bicarbonate and carbonate concentrations and the total concentration of Na^+ in the electrolyte (Figure 3). Predictably, the largest changes occur in the 0.25 M $NaHCO_3$ solution in which $[HCO_3^-]$ near the electrode decreases by 19% at −0.9 V. For comparison, the decreases in $[HCO_3^-]$ are 12, 5, and 8% for unstirred 0.5 M and stirred 0.5 M and 1.0 M $NaHCO_3$, respectively. Perhaps most importantly, assuming all species reach equilibrium, $[CO_{2(aq)}]$ decreases by an order of magnitude at −0.7 V and falls to under 3 mM in each case at −0.9 V. It is important to note that, although the equilibrium between carbonate and bicarbonate is sufficiently fast to reach equilibrium under reaction conditions, the hydration of CO_2 is significantly slower and therefore the equilibrium assumption may not hold for

DOI: 10.1021/acscatal.8b01032
ACS Catal. 2018, 8, 3999−4008

$[CO_{2(aq)}]$.[6,37,39] The validity of this assumption was tested using ATR-SEIRAS to monitor $[CO_{2(aq)}]$ as a function of potential from 0.0 to −0.9 V in 0.5 M $NaHCO_3$ with and without stirring as described in the Materials and Methods. It was found that, although the calculated $[CO_{2(aq)}]$ only slightly underestimates the experimentally observed value without stirring (Figure 4a), $[CO_{2(aq)}]$ remains roughly constant from 0.0 to −0.9 V when the electrolyte is stirred (Figure 4b). This result suggests that, although $CO_{2(aq)}$ nearly reaches equilibrium without stirring, when stirring is introduced, transport of $CO_{2(aq)}$ to the electrode is faster than the conversion of $CO_{2(aq)}$ to bicarbonate so that $[CO_{2(aq)}]$ remains constant at all potentials tested. Additional tests at stirring rates of 450, 900, 1350, and 1800 rpm at −0.7 V suggest that even stirring at 450 rpm is sufficient to maintain a $[CO_{2(aq)}]$ equal to that of the bulk value (Figure S7). It is important to emphasize that, due to the dependence of $[CO_{2(aq)}]$ on stirring rate, spectroscopic data should not be correlated with reactivity data without maintaining a similar level of convection. As a result, the relationship established by Ayemoba et al. between decreased near-electrode pH and improved CO_2RR selectivity (which was determined based on the relative ratio of $CO_{2(aq)}$ and bicarbonate peaks in an unstirred spectroscopic cell)[2] on Cu electrodes must be reevaluated with more rigorous control of convection during spectroscopic measurements.

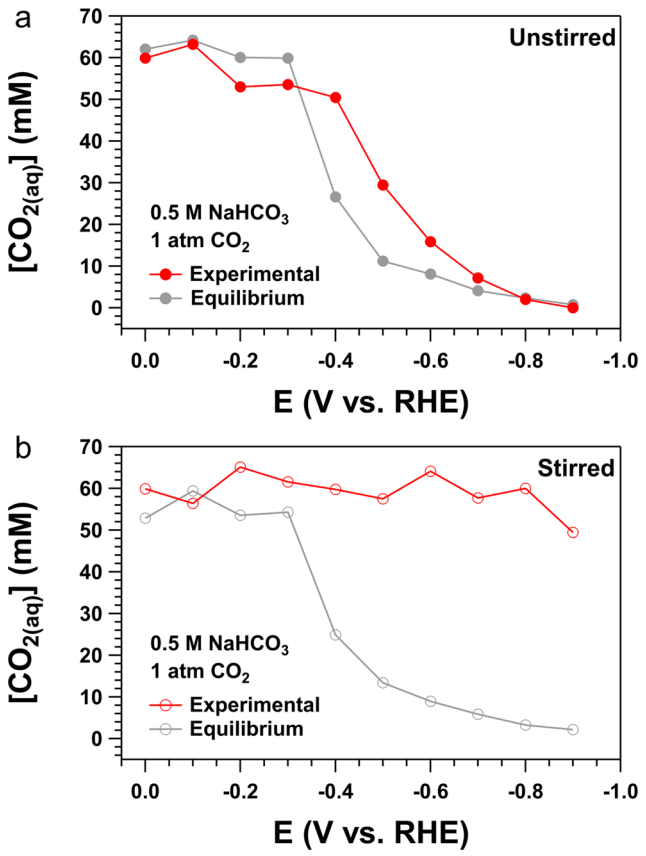

Figure 4. Calculated (gray) and measured $CO_{2(aq)}$ near-surface concentrations (a) with no stirring and (b) stirred at 1800 rpm in CO_2-saturated 0.5 M $NaHCO_3$ versus uncorrected potential. Experimental values taken from the spectra in Figure S2.

Similar to the depletion of protons, the depletion of $CO_{2(aq)}$ near the electrode in the unstirred case yields an additional concentration overpotential (η_{c,CO_2}), further limiting the efficiency of the CO_2RR at lower potentials. Solving eq 1 with the experimentally determined interfacial $[CO_{2(aq)}]$ values given in Figure 4, η_{c,CO_2} is smaller than η_{c,H^+} at lower overpotential but reaches nearly the same value (87 and 82 mV, respectively) at −0.8 V in unstirred 0.5 M $NaHCO_3$ (Figure 5). As a result, the total concentration overpotential ($\eta_{c,total}$) increases from 123 mV at −0.7 V to 169 mV at −0.8 V so that 46 mV of the additional 100 mV of overpotential is wasted due to transport limitations. This additional η_c could be a key factor in understanding the decrease in CO_2RR selectivity relative to the HER at high overpotentials.[45] Whereas the HER is only susceptible to η_{c,H^+}, the CO_2RR is subject to both η_{c,H^+} and η_{c,CO_2} so that from −0.7 to −0.8 V the additional kinetic overpotentials for CO_2RR and HER are 54 and 86 mV, respectively. It is important to note, however, that this analysis is applicable to the unstirred case only as the $[CO_{2(aq)}]$ stays roughly constant from 0.0 to −0.9 V in the stirred case (Figure 4b) so that no η_{c,CO_2} is observed and the relative increases in kinetic overpotential with electrode potential are expected to be the same for CO_2RR and HER within the potential range studied in this work. η_{c,CO_2} is not calculated beyond −0.8 V because $[CO_{2(aq)}]$ decreases below the detection limit of ATR-SEIRAS so that eq 1 diverges toward infinity when the near-electrode $[CO_{2(aq)}]$ goes to 0 M.

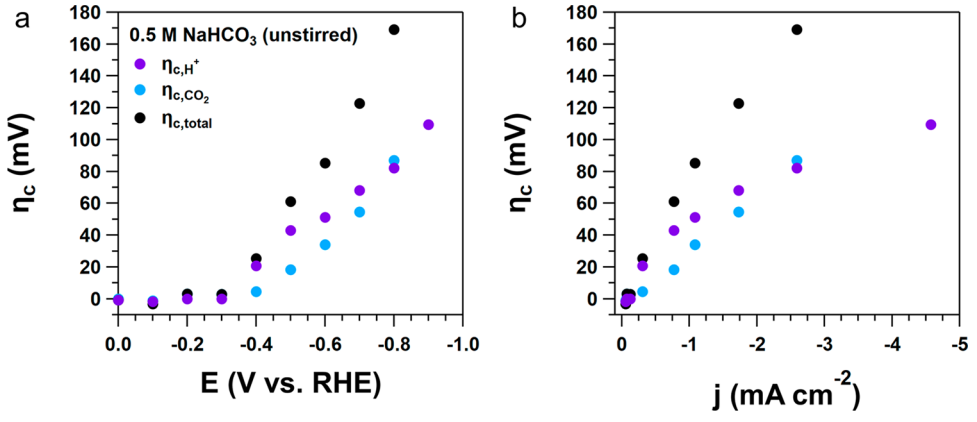

Figure 5. η_{c,H^+} (purple), η_{c,CO_2} (blue), and $\eta_{c,total}$ (black) as a function of (a) electrode potential and (b) current density in CO_2-saturated 0.5 M $NaHCO_3$ without stirring.

DOI: 10.1021/acscatal.8b01032
ACS Catal. 2018, 8, 3999−4008

The findings discussed above are particularly insightful for understanding the electrocatalytic performances of high-surface area electrodes for CO_2 reduction. When nanostructured catalysts are employed, the localized concentration gradients are expected to be much more substantial than on the planar electrodes. The current densities for the nanostructured electrodes can typically reach the scale of 10 mA/cm^2 (per geometric area of the electrode) or above[18,34,46−48] with the estimated η_{c,H^+} upward of 100 mV[28] (Figure 2). Moreover, the diffusion of chemical species inside the nanostructured electrodes can be expected to be slower than that from the bulk electrolyte toward the surface of a planar electrode, which is likely closer to the unstirred case in the absence of convection flow investigated in this work (Figure 4a), and $CO_{2(aq)}$ can be depleted in a significant part of the electrodes at elevated potentials or current densities. The drastic difference in $CO_{2(aq)}$ concentration between the unstirred and stirred situations shown in Figure 4 thus underlines the need for taking the mass transport effects into account in the design and evaluation of nanostructured electrodes.

Kinetic Implications. These observed decreases in reactant concentrations, along with the corresponding increase in η_c, have significant impacts on the interpretation of kinetic analysis of electrochemical systems.[6] For example, CO_2 reduction to CO exhibits a Tafel slope of 56 mV dec^{-1} in the lower overpotential region (> −0.4 V), which increases to 250 mV dec^{-1} at higher overpotential (< −0.5 V; Figure 6, solid circles).[33] We have previously attributed the change in Tafel slope to mass transport limitations of reactants ($CO_{2(aq)}$ and bicarbonate) or site blocking due to Na^+ in the outer Helmholtz plane at negatively charged electrodes. It is interesting to note, however, that the shift in slope occurs concurrently with the onset of η_{c,H^+} at −0.4 V, suggesting that elevation of interfacial concentration gradients may be a cause of the shifting Tafel slope. Using η_{c,H^+} values from the stirred cell in 0.5 M $NaHCO_3$, the potential in the Tafel plot was corrected to account for current-induced concentration gradients by subtracting η_{c,H^+} from the electrode potential, yielding a mass-transport free potential. The η_{c,H^+} corrected Tafel plot can be used to examine the effect of interfacial concentration gradients on existing kinetic data (Figure 6, open circles). Although the increase in η_{c,H^+} does not account entirely for the shift, the slope of the high overpotential region decreases from 250 to 224 mV dec^{-1}, indicating that mass transport limitations do have a minor, yet measurable, effect on the kinetics of CO_2 reduction to CO on Au. Moreover, we can also rule out η_{c,CO_2} as the primary cause of shifting Tafel slope. Within the potential range studied in the Tafel analysis (−0.3 to −0.7 V), there is no significant change in $[CO_{2(aq)}]$ while stirring (the same conditions under which the Tafel slope was determined) based on ATR-SEIRAS measurements. As a result, we conclude that, although a small part of the shift in slope can be attributed to η_{c,H^+} changes, the major cause is the blocking of active sites by Na^+, as detailed in our previous work.[33,49]

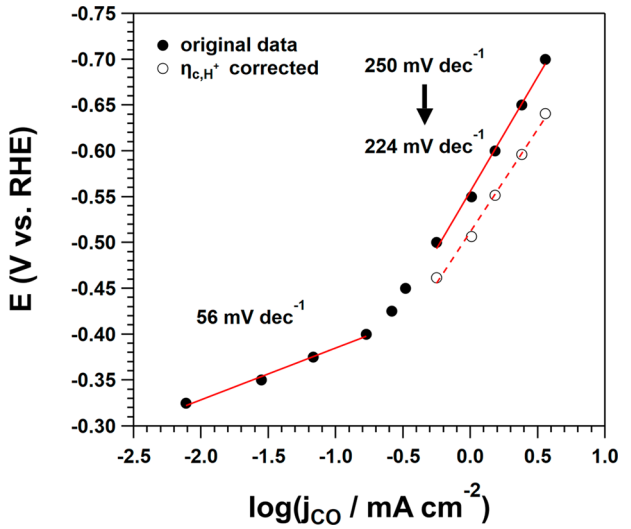

Figure 6. Uncorrected (solid circles) and η_{c,H^+} corrected (open circles) Tafel slope for the CO_2RR to CO in CO_2-saturated 0.5 M $NaHCO_3$. Data taken from ref 33.

In addition to impacting the Tafel slope, η_{c,H^+} will also impact reaction order studies of electrochemical systems. For example, increases in current density with reactant concentration (and corresponding increases in η_{c,H^+}) lead to growing overestimations of the kinetic overpotential at higher concentrations. If the overestimation of kinetic overpotential on the surface increases with current density (and overpotential) in concentration-dependence investigations, the obtained reaction order dependence on that species will be underestimated relative to the true value. To obtain a strictly accurate dependence, the η_{c,H^+} should be determined at each concentration, and measurements should be repeated iteratively to account for η_{c,H^+}. We will illustrate this point with a simple model reaction in which hydroxide is produced at the cathode (eq 3).

$$A + H_2O + e^- \rightarrow B + OH^- \quad (3)$$

Assuming the rate of this reduction reaction has a first order dependence on species A, in the absence of near-electrode concentration gradients, a slope of ∼1 when plotting log(j) vs log[A] should be observed experimentally at a constant potential (or overpotential). However, misleading electrokinetic data could be obtained if there is substantial contribution from η_{c,H^+}. This point will be shown at current densities below 6 mA/cm^{-2}, where we have experimentally determined η_{c,H^+} (Figure 3b), and is a commonly used current density range for reaction order dependence studies.[33,34,47] When η_{c,H^+} = 0, a slope of 1 is obtained (Figure 7, red line) as expected from the assumption. When η_{c,H^+} > 0, overpotential will be overestimated based on the η_{c,H^+}−current density relationship established for the stirred 0.5 M $NaHCO_3$ (Figure 2b). Current densities are then recalculated with a given Tafel slope at the η_{c,H^+} corrected overpotential (E − η_{c,H^+}, Figure S8). This process is repeated until the predicted η_{c,H^+} converges (change in η_{c,H^+} < 1 mV between iterations). For reactions with Tafel slopes of 236, 118, and 59 mV dec^{-1}, the observed dependence on [A] (without correcting for η_{c,H^+}) decreases from 1 to 0.83, 0.71, and 0.55, respectively (Figure 7). The sequence is consistent with the fact that a lower Tafel slope entails a more pronounced effect of a given η_{c,H^+} on the current. Such discrepancies in reaction orders can cause severe errors in mechanistic interpretation of electrochemical processes. For example, if the model reaction has a Tafel slope of 59 mV dec^{-1}, the reaction will appear to be roughly half order, rather than first order in [A]. In light of these results, it is imperative that all studies of reaction order dependence are conducted at a minimal overpotential (to minimize concentration gradients)

DOI: 10.1021/acscatal.8b01032
ACS Catal. 2018, 8, 3999−4008

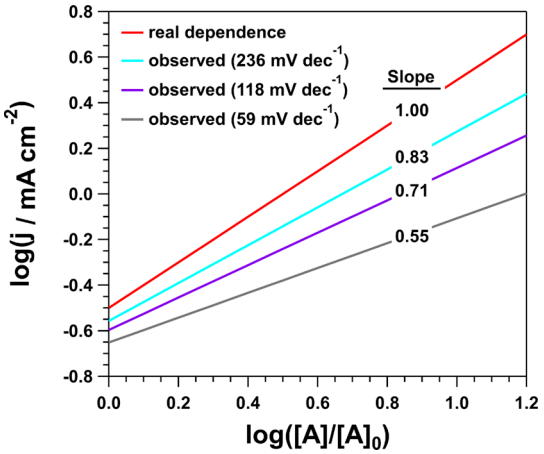

Figure 7. Theoretical (red) and expected experimentally observed reaction order dependence on species *A* based on overpotential underestimation for the sample reaction given in eq 2 with a Tafel slopes of 236 mV dec^{-1} (light blue), 118 mV dec^{-1} (purple), and 59 mV dec^{-1} (gray). Overpotential changes calculated based on η_{c,H^+}–current density relationship in stirred 0.5 M $NaHCO_3$.

with facile mass transport and a strong buffer to minimize the deviation of the kinetic overpotential caused by η_{c,H^+}.

The methodology outlined here may also be used for the study of concentration gradient changes in a wide variety of electrochemical processes provided the electrolyte contains a multiprotic salt, and the electrode of interest can provide a surface-sensitive film. For example, the interfacial concentrations of a phosphate electrolyte can be quantified by examining the relative ratio of PO_4^{3-}, HPO_4^{2-}, and $H_2PO_4^-$ bands. The results of such experiments could have important implications, as demonstrated here for CO_2 reduction, for other widely studied electrochemical processes such as hydrogen oxidation or nitrate reduction.

CONCLUSIONS

Changes in interfacial concentrations and the resultant increases in concentration overpotential arising from production of OH^- during the HER and CO_2RR were quantified experimentally with ATR-SEIRAS under nonstirred and stirred conditions. Increases in η_{c,H^+} as a function of current in CO_2-saturated 0.25, 0.5, and 1.0 M $NaHCO_3$ electrolytes occurs at rates of 93, 68, and 48 mV per decade of current density, respectively, for unstirred electrolytes, and 48 mV per decade in 0.5 M $NaHCO_3$ when stirred at 1800 rpm. These trends can be applied directly to studies of the CO_2RR on any flat electrode, as the η_{c,H^+} is only dependent on the production rate of OH^- rather than the product distribution or the composition of the electrode surface. Although the quantitative relationships given here should serve as close approximations to the interfacial behavior on other electrodes, exact quantitative relationships should be established for each electrode material and morphology using the methods detailed in this work. Increases in η_{c,H^+} have a strong effect on CO_2RR rates via two different mechanisms: (1) overestimation of applied kinetic overpotential due to $[H^+]$ gradients and (2) depletion of $CO_{2(aq)}$ near the electrode via equilibrium reactions with hydroxide and carbonate anions, resulting in an additional concentration overpotential for $CO_{2(aq)}$. Although improvement of mass transport has a limited mitigating effect on the first mechanism, in this study it was found that, with sufficient convection, the effect of the second mechanism can be eliminated within the current range studied due to the slow hydration of CO_2 relative to other equilibrium reactions. Therefore, improvements in selectivity of the CO_2RR over the HER can be made by operating at high current densities with sufficient mass transport of $CO_{2(aq)}$. Additionally, it is necessary for future mechanistic work to more carefully consider the effect of concentration overpotentials either through experimental quantification of η_c or by operating under conditions in which η_c is negligible, e.g., low current densities and/or a strong buffer, to avoid misleading electrokinetic data.

ASSOCIATED CONTENT

Supporting Information

The Supporting Information is available free of charge on the ACS Publications website at DOI: 10.1021/acscatal.8b01032.

Raw spectra and peak fits, plots of surface pH versus electrode potential and current density, and CO_2 IR band intensities at different stir rates (PDF)

AUTHOR INFORMATION

Corresponding Authors

*E-mail: yays@udel.edu.
*E-mail: bxu@udel.edu.

ORCID

Yushan Yan: 0000-0001-6616-4575
Bingjun Xu: 0000-0002-2303-257X

Notes

The authors declare no competing financial interest.

ACKNOWLEDGMENTS

The authors thank the Keck Center for Advanced Microscopy and Microanalysis for help with SEM imaging as well as the University of Delaware College of Engineering Machine Shop for fabrication of all custom spectroelectrochemical cells. We also thank Professor Chao Wang from Johns Hopkins University for helpful discussion of the effect of surface pH changes on nanostructured materials. B.X. acknowledges the support of National Science Foundation CAREER Program (Award No. CBET-1744586). M.D. and Y.Y. acknowledge the support of the National Science Foundation–Chemical Catalysis Program (Award No. CHE-1566138).

REFERENCES

(1) Bard, A. J.; Faulkner, L. R. *Electrochemical Methods: Fundamentals and Applications*; Wiley, 2000.
(2) Ayemoba, O.; Cuesta, A. Spectroscopic Evidence of Size-Dependent Buffering of Interfacial pH by Cation Hydrolysis during CO_2 Electroreduction. *ACS Appl. Mater. Interfaces* **2017**, *9*, 27377–27382.
(3) Carneiro-Neto, E. B.; Lopes, M. C.; Pereira, E. C. Simulation of Interfacial pH Changes during Hydrogen Evolution Reaction. *J. Electroanal. Chem.* **2016**, *765*, 92–99.
(4) Chang, Y.-C.; Prentice, G. Calculation of pH Near the Surface of an Electrode Covered with a Porous Film. *Electrochim. Acta* **1986**, *31*, 579–584.
(5) Deligianni, H.; Romankiw, L. T. In-Situ Surface pH Measurement during Electrolysis using a Rotating pH Electrode. *IBM J. Res. Dev.* **1993**, *37*, 85–95.
(6) Gupta, N.; Gattrell, M.; MacDougall, B. Calculation for the Cathode Surface Concentrations in the Electrochemical Reduction of CO_2 in $KHCO_3$ Solutions. *J. Appl. Electrochem.* **2006**, *36*, 161–172.

DOI: 10.1021/acscatal.8b01032
ACS Catal. 2018, 8, 3999–4008

(7) Henstridge, M. C.; Wildgoose, G. G.; Compton, R. G. Generator/Collector Experiments with a Single Electrode: Introduction and Application to Exploring the Oxidation Mechanism of Serotonin. *J. Phys. Chem. C* **2009**, *113*, 14285−14289.
(8) Henstridge, M. C.; Wildgoose, G. G.; Compton, R. G. Generator−Collector Experiments at a Single Electrode: Exploring the General Applicability of This Approach by Comparing the Performance of Surface Immobilized versus Solution Phase Sensing Molecules. *Langmuir* **2010**, *26*, 1340−1346.
(9) Hori, Y. Electrochemical CO_2 Reduction on Metal Electrodes. In *Modern Aspects of Electrochemistry*, Vayenas, C., White, R., Gamboa-Aldeco, M., Eds.; Springer: New York, 2008; Vol. *42*, pp 89−189.
(10) Hotta, H.; Tatsuno, K.; Hattori, Y.; Hashimoto, T.; Uehara, M.; Tsunoda, K.-i. In-Situ Monitoring of the H^+Concentration Change Near an Electrode Surface through Electrolysis using Slab Optical Waveguide pH Sensor. *Electrochem. Commun.* **2008**, *10*, 1351−1354.
(11) Ji, J.; Cooper, W. C.; Dreisinger, D. B.; Peters, E. Surface pH Measurements during Nickel Electrodeposition. *J. Appl. Electrochem.* **1995**, *25*, 642−650.
(12) Katsounaros, I.; Meier, J. C.; Klemm, S. O.; Topalov, A. A.; Biedermann, P. U.; Auinger, M.; Mayrhofer, K. J. J. The Effective Surface pH during Reactions at the Solid−Liquid Interface. *Electrochem. Commun.* **2011**, *13*, 634−637.
(13) Kuhn, A. T.; Chan, C. Y. pH Changes at Near-Electrode Surfaces. *J. Appl. Electrochem.* **1983**, *13*, 189−207.
(14) Lim, C. F. C.; Harrington, D. A.; Marshall, A. T. Effects of Mass Transfer on the Electrocatalytic CO_2Reduction on Cu. *Electrochim. Acta* **2017**, *238*, 56−63.
(15) Martínez-Hincapié, R.; Sebastián-Pascual, P.; Climent, V.; Feliu, J. M. Exploring the Interfacial Neutral pH Region of Pt(111) Electrodes. *Electrochem. Commun.* **2015**, *58*, 62−64.
(16) Pickering, H. W. The Significance of the Local Electrode Potential within Pits, Crevices and Cracks. *Corros. Sci.* **1989**, *29*, 325−341.
(17) Raciti, D.; Cao, L.; Livi, K. J. T.; Rottmann, P. F.; Tang, X.; Li, C.; Hicks, Z.; Bowen, K. H.; Hemker, K. J.; Mueller, T.; Wang, C. Low-Overpotential Electroreduction of Carbon Monoxide Using Copper Nanowires. *ACS Catal.* **2017**, *7*, 4467−4472.
(18) Raciti, D.; Livi, K. J.; Wang, C. Highly Dense Cu Nanowires for Low-Overpotential CO_2 Reduction. *Nano Lett.* **2015**, *15*, 6829−6835.
(19) Santos, J. S.; Matos, R.; Trivinho-Strixino, F.; Pereira, E. C. Effect of Temperature on Co Electrodeposition in the Presence of Boric Acid. *Electrochim. Acta* **2007**, *53*, 644−649.
(20) Santos, J. S.; Trivinho-Strixino, F.; Pereira, E. C. Investigation of $Co(OH)_2$Formation during Cobalt Electrodeposition using a Chemometric Procedure. *Surf. Coat. Technol.* **2010**, *205*, 2585−2589.
(21) Singh, M. R.; Kwon, Y.; Lum, Y.; Ager, J. W.; Bell, A. T. Hydrolysis of Electrolyte Cations Enhances the Electrochemical Reduction of CO_2 over Ag and Cu. *J. Am. Chem. Soc.* **2016**, *138*, 13006−13012.
(22) Soffer, A.; Folman, M. The Electrical Double Layer of High Surface Porous Carbon Electrode. *J. Electroanal. Chem. Interfacial Electrochem.* **1972**, *38*, 25−43.
(23) Strbac, S. The Effect of pH on Oxygen and Hydrogen Peroxide Reduction on Polycrystalline Pt Electrode. *Electrochim. Acta* **2011**, *56*, 1597−1604.
(24) Yang, Y.-F.; Denuault, G. Scanning Electrochemical Microscopy (SECM) Study of pH Changes at Pt Electrode Surfaces in Na_2SO_4Solution (pH 4) under Potential Cycling Conditions. *J. Chem. Soc., Faraday Trans.* **1996**, *92*, 3791−3798.
(25) Hori, Y.; Murata, A.; Takahashi, R. Formation of Hydrocarbons in the Electrochemical Reduction of Carbon Dioxide at a Copper Electrode in Aqueous Solution. *J. Chem. Soc., Faraday Trans. 1* **1989**, *85*, 2309−2326.
(26) Raciti, D.; Mao, M.; Wang, C. Mass Transport Modelling for the Electroreduction of CO_2 on Cu Nanowires. *Nanotechnology* **2018**, *29*, 044001.
(27) Singh, M. R.; Clark, E. L.; Bell, A. T. Effects of Electrolyte, Catalyst, and Membrane Composition and Operating Conditions on the Performance of Solar-Driven Electrochemical Reduction of Carbon Dioxide. *Phys. Chem. Chem. Phys.* **2015**, *17*, 18924−18936.
(28) Kas, R.; Kortlever, R.; Yılmaz, H.; Koper, M. T. M.; Mul, G. Manipulating the Hydrocarbon Selectivity of Copper Nanoparticles in CO_2 Electroreduction by Process Conditions. *ChemElectroChem* **2015**, *2*, 354−358.
(29) Osawa, M. Dynamic Processes in Electrochemical Reactions Studied by Surface-Enhanced Infrared Absorption Spectroscopy (SEIRAS). *Bull. Chem. Soc. Jpn.* **1997**, *70*, 2861−2880.
(30) Osawa, M. Surface-Enhanced Infrared Absorption. In *Near-Field Optics and Surface Plasmon Polaritons*; Kawata, S., Ed.; Springer: Berlin, Heidelberg, 2001; Vol. *81*, pp 163−187.
(31) Osawa, M.; Ataka, K.-i.; Yoshii, K.; Yotsuyanagi, T. Surface-Enhanced Infrared ATR Spectroscopy for In-Situ Studies of Electrode/Electrolyte Interfaces. *J. Electron Spectrosc. Relat. Phenom.* **1993**, *64*−*65*, 371−379.
(32) Osawa, M.; Ikeda, M. Surface-Enhanced Infrared Absorption of p-Nitrobenzoic Acid Deposited on Silver Island Films: Contributions of Electromagnetic and Chemical Mechanisms. *J. Phys. Chem.* **1991**, *95*, 9914−9919.
(33) Dunwell, M.; Lu, Q.; Heyes, J. M.; Rosen, J.; Chen, J. G.; Yan, Y.; Jiao, F.; Xu, B. The Central Role of Bicarbonate in the Electrochemical Reduction of Carbon Dioxide on Gold. *J. Am. Chem. Soc.* **2017**, *139*, 3774−3783.
(34) Chen, Y.; Li, C. W.; Kanan, M. W. Aqueous CO2 Reduction at Very Low Overpotential on Oxide-Derived Au Nanoparticles. *J. Am. Chem. Soc.* **2012**, *134* (49), 19969−19972.
(35) Wuttig, A.; Surendranath, Y. Impurity Ion Complexation Enhances Carbon Dioxide Reduction Catalysis. *ACS Catal.* **2015**, *5*, 4479−4484.
(36) Arihara, K.; Kitamura, F.; Ohsaka, T.; Tokuda, K. Characterization of the Adsorption state of Carbonate Ions at the Au(111) Electrode Surface using In-Situ IRAS. *J. Electroanal. Chem.* **2001**, *510*, 128−135.
(37) Pinsent, B. R. W.; Pearson, L.; Roughton, F. J. W. The Kinetics of Combination of Carbon Dioxide with Hydroxide Ions. *Trans. Faraday Soc.* **1956**, *52*, 1512−1520.
(38) Pocker, Y.; Bjorkquist, D. W. Stopped-Flow Studies of Carbon Dioxide Hydration and Bicarbonate Dehydration in $H_2O$and D_2O. Acid-base and Metal Ion Catalysis. *J. Am. Chem. Soc.* **1977**, *99*, 6537−6543.
(39) Schulz, K. G.; Riebesell, U.; Rost, B.; Thoms, S.; Zeebe, R. E. Determination of the Rate Constants for the Carbon Dioxide to Bicarbonate Inter-Conversion in pH-Buffered Seawater Systems. *Mar. Chem.* **2006**, *100*, 53−65.
(40) Kuhl, K. P.; Hatsukade, T.; Cave, E. R.; Abram, D. N.; Kibsgaard, J.; Jaramillo, T. F. Electrocatalytic Conversion of Carbon Dioxide to Methane and Methanol on Transition Metal Surfaces. *J. Am. Chem. Soc.* **2014**, *136*, 14107.
(41) Peterson, A. A.; Nørskov, J. K. Activity Descriptors for CO_2 Electroreduction to Methane on Transition-Metal Catalysts. *J. Phys. Chem. Lett.* **2012**, *3*, 251−258.
(42) Rosen, J.; Hutchings, G. S.; Lu, Q.; Rivera, S.; Zhou, Y.; Vlachos, D. G.; Jiao, F. Mechanistic Insights into the Electrochemical Reduction of CO_2 to CO on Nanostructured Ag Surfaces. *ACS Catal.* **2015**, *5*, 4293−4299.
(43) Sheng, W.; Kattel, S.; Yao, S.; Yan, B.; Liang, Z.; Hawxhurst, C.; Wu, Q.; Chen, J. G. Electrochemical Reduction of CO2 to Synthesis Gas with Controlled CO/H_2 Ratios. *Energy Environ. Sci.* **2017**, *10*, 1180.
(44) Zhu, W.; Michalsky, R.; Metin, Ö.; Lv, H.; Guo, S.; Wright, C. J.; Sun, X.; Peterson, A. A.; Sun, S. Monodisperse Au Nanoparticles for Selective Electrocatalytic Reduction of CO_2 to CO. *J. Am. Chem. Soc.* **2013**, *135*, 16833−16836.
(45) Hori, Y.; Murata, A.; Kikuchi, K.; Suzuki, S. Electrochemical Reduction of Carbon Dioxides to Carbon Monoxide at a Gold Electrode in Aqueous Potassium Hydrogen Carbonate. *J. Chem. Soc., Chem. Commun.* **1987**, 728−729.

DOI: 10.1021/acscatal.8b01032
ACS Catal. 2018, 8, 3999−4008

(46) Li, C. W.; Kanan, M. W. CO_2 Reduction at Low Overpotential on Cu Electrodes Resulting from the Reduction of Thick Cu_2O Films. *J. Am. Chem. Soc.* **2012**, *134*, 7231−7234.
(47) Lu, Q.; Rosen, J.; Zhou, Y.; Hutchings, G. S.; Kimmel, Y. C.; Chen, J. G.; Jiao, F. A Selective and Efficient Electrocatalyst for Carbon Dioxide Reduction. *Nat. Commun.* **2014**, *5*, 3242.
(48) Mistry, H.; Varela, A. S.; Bonifacio, C. S.; Zegkinoglou, I.; Sinev, I.; Choi, Y.-W.; Kisslinger, K.; Stach, E. A.; Yang, J. C.; Strasser, P.; Cuenya, B. R. Highly Selective Plasma-Activated Copper Catalysts for Carbon Dioxide Reduction to Ethylene. *Nat. Commun.* **2016**, *7*, 12123.
(49) Dunwell, M.; Wang, J.; Yan, Y.; Xu, B. Surface Enhanced Spectroscopic Investigations of Adsorption of Cations on Electrochemical Interfaces. *Phys. Chem. Chem. Phys.* **2017**, *19*, 971−975.

DOI: 10.1021/acscatal.8b01032
ACS Catal. 2018, 8, 3999−4008